Intriguing Properties of Modern GANs

Roy Friedman
Department of Computer Science
Hebrew University of Jerusalem

roy.friedman@mail.huji.ac.il

Yair Weiss
Department of Computer Science
Hebrew University of Jerusalem

Abstract

Modern GANs achieve remarkable performance in terms of generating realistic and diverse samples. This has led many to believe that "GANs capture the training data manifold". In this work we show that this interpretation is wrong. We empirically show that the manifold learned by modern GANs does not fit the training distribution: specifically the manifold does not pass through the training examples and passes closer to out-of-distribution images than to in-distribution images. We also investigate the distribution over images implied by the prior over the latent codes and study whether modern GANs learn a density that approximates the training distribution. Surprisingly, we find that the learned density is very far from the data distribution and that GANs tend to assign higher density to out-of-distribution images. Finally, we demonstrate that the set of images used to train modern GANs are often not part of the typical set described by the GANs' distribution.

1 Introduction

Starting with their original formulation, Generative Adversarial Networks (GANs, Goodfellow et al. 2014) quickly gained enormous popularity. As their popularity increased, so did the approaches to evaluating the quality of the images created by GANs and their fidelity to the true distribution (e.g. Heusel et al. 2017; Richardson & Weiss 2018; Arora et al. 2018; Kynkäänniemi et al. 2019). These methods exposed many problems in the distributions of images generated by GANs, such as mode collapse (Goodfellow 2016 and artifacts within generated images (Karras et al. 2021). Such developments were carried out with the understanding that "the GAN's training criteria has a global minimum at the true distribution" (from Theorem 1 of Goodfellow et al.).

Following these evaluations, there was a refinement of GANs and such failures have become much less prominent. For example, FID (Heusel et al. 2017) and recall (Kynkäänniemi et al. 2019) both check whether the full diversity of the training distribution is captured by the generative model. GANs which have both low FID and high recall are deemed not to suffer from mode collapse, as they supposedly capture the full support of the training data. Due to their impressive performance in such metrics, many applications have progressed with a working assumption that GANs learn the "training data manifold" (Schlegl et al. 2017) This assumption has even carried through to domains where an incorrect model of the true distribution can incur heavy risks, such as super-resolving MRI scans (Bendel et al. 2022), simulations for self-driving cars (Zhang et al. 2018a), detecting cancer through GAN inversions (Schlegl et al. 2017), recovering frequencies in astrophysical images (Schawinski et al. 2017) and more.

In this work we study GANs with excellent performance and question whether these GANs have actually learned the true data manifold. By critically analyzing GANs through this lens, we find that they behave in ways counter to popular belief.

As mentioned above, modern GANs are frequently thought of as manifold methods, wherein the GANs' generator captures the image manifold. Surprisingly, we find that training examples are not part of the

learned manifold. We go on to demonstrate that the GAN manifold passes almost the same distance from the class of images the generator was trained on as other classes, even when measured with a perceptual distance (Zhang et al. 2018b). This failure is intriguing as a GAN trained on ships, for instance, is only able to generate images of ships and not other object classes. Furthermore, we find that the GAN manifold passes unusually close to images outside the training domain. In particular, we show that the GAN manifold passes closer to SVHN images than to the images it was trained on.

While GANs are most commonly viewed as manifold methods, we demonstrate how analyzing them only in these terms might not capture the full breadth of their capabilities. In particular, the manifold view ignores the density the generator assigns to different parts of space and whether or not the manifold is more abundant in regions around the true distribution. To account for this, we analyze the density the GAN's generator assigns to samples in terms of the average test log-likelihood. While mostly overlooked in the GAN literature, the log-likelihood is widely used to evaluate other families of generative models, such as score based models (Song et al. 2020) and normalizing flows (Kingma & Dhariwal 2018). Moreover, the log-likelihood was used in the past to show that large families of generative models assign higher likelihood to images outside the training distribution than those used in training (Nalisnick et al. 2018) and that many conditional generative models are weak classifiers (Fetaya et al. 2019). Works such as those by Nalisnick et al. focused on models where the likelihood is tractable, which have much worse FID scores than modern GANs. There is scarce literature of this vein concerning generative models that show excellent results on metrics other than average test log-likelihood.

By evaluating GANs with low FID as density estimators, we show that modern GANs under-perform in terms of average test log-likelihood when compared to models with much worse FID. We go on to show that GANs are biased towards images with larger "flat" areas. Indeed, the log-likelihood assigned by the GAN is anti-correlated with local variance in the image. Finally, we question whether the images used to train the GAN are part of the typical set of images, a test previously used to determine whether a set of images are outliers according to a generative model (Nalisnick et al. 2019).

To summarize, in this paper we discuss four intriguing properties of modern GANs:

- The learned manifold does not pass through the training examples.

- The learned manifold is closer to out-of-distribution images than to in-distribution images.

- The density model learned by by the GAN assigns higher density to out-of-distribution images.

- The training images are not in the typical set of the GAN.

2 Background

2.1 Evaluation of Generative Models

State of the art GANs (Sauer et al. 2022; Karras et al. 2020b; Kang et al. 2023) are typically evaluated by methods that analyze the statistics of the generated samples (Heusel et al. 2017; Kynkäänniemi et al. 2019; Richardson & Weiss 2018). Almost all of these approaches define a statistic that is zero only if the GAN-generated and true samples are from the same distribution. Methods such as these are extremely effective in determining whether the generative model has learned the correct statistic but are somewhat limited. One such limitation is that for data in very high dimensions, many samples might be needed to determine if the true and generated distribution are distinct. Another is that the difference between the distributions is only measured on particular statistics, ignoring the others.

Many generative models other than GANs utilize the average test log-likelihood (LL) as an additional evaluation metric, since high test LL is equivalent to low KL divergence between the generative distribution and the true data distribution. For example, score-based models (Song et al. 2020) and normalizing flows (Kingma & Dhariwal 2018; Nalisnick et al. 2018; Fetaya et al. 2019) report the test LL or the negative test LL as a way to compare the quality of the model. Since the LL is never explicitly used in GANs, it was
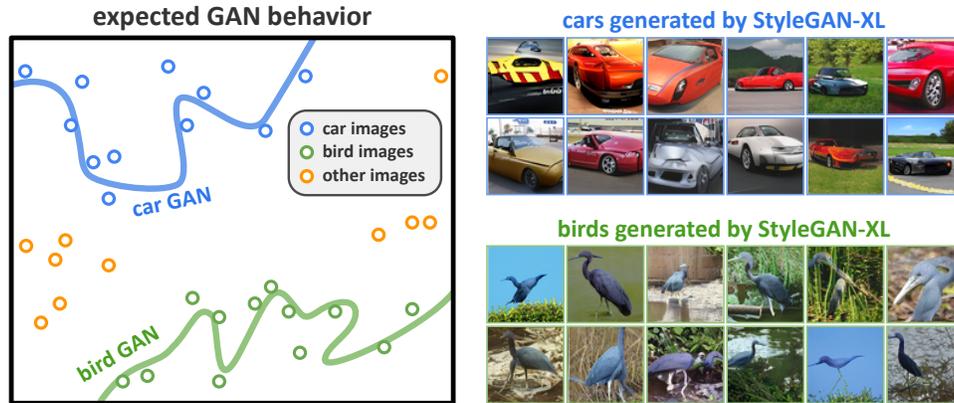
Figure 1: Modern GANs work amazingly well, to the point that it is expected that they capture the data manifold (left). It is typically assumed that because GANs can generate realistic images (right) that they capture the true data manifold. In this paper we show that this assumption is false.
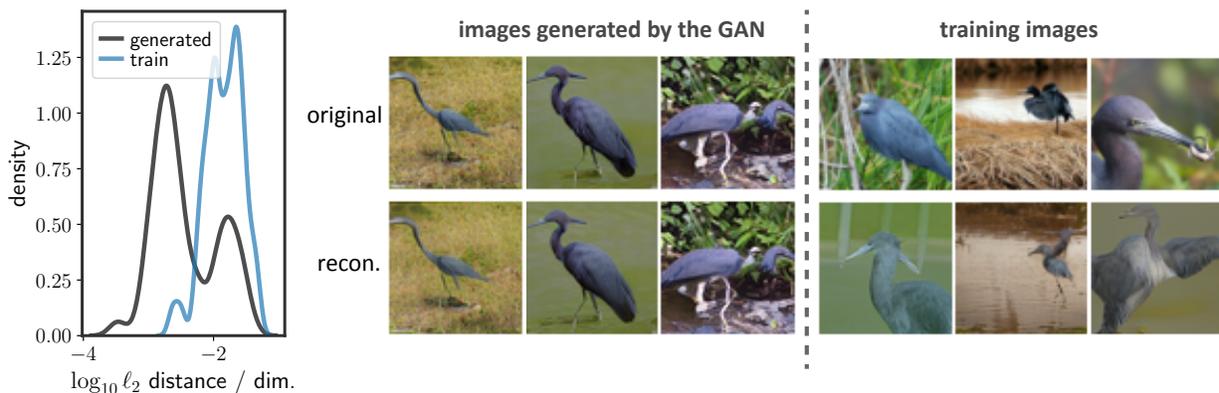

Figure 2: **Left:** ℓ_2 distance (lower is better) of reconstructions of generated and train images under StyleGAN-XL (Sauer et al. 2022) trained on ImageNet (when only z is optimized). The distribution of reconstruction errors for training images is distinct from the same for images generated by the GAN, implying that the training images are not part of the GAN manifold. **Right:** examples of projections to the GAN. Generated images are part of the manifold (and can be reconstructed), but training images are not. For training images, the reconstructed images are realistic birds but they are different birds.

largely ignored when comparing such models and calculated in only relatively few studies for small scale models on simple images, such as MNIST (Wu et al. 2016; Theis et al. 2015).

In the past, generative models were also evaluated through their performance in inference tasks, such as generative classification (e.g. Fetaya et al. 2019; Hinton et al. 1995). In generative classification, a generative model $p_{\theta_c}(x|c)$ is separately trained for each class c in the data. An unseen sample is then classified by determining which class-conditional LL is the largest:

$$\hat{c}(x) = \arg\max_c \log p_{\theta_c}(x|c) \tag{1}$$

where $\hat{c}(x)$ is the predicted class for sample x. If $p_{\theta_c}(x|c) \approx p_{\text{data}}(x|c)$ for all classes c, then the above classification scheme is guaranteed to be optimal (Duda et al. 1973). On the flip side, if the classification performance is sub-optimal, then in no uncertain terms $p_{\theta_c}(x|c) \neq p_{\text{data}}(x|c)$. Using inference tasks to evaluate generative models can expose biases in the generative distribution, and is potentially a sample-efficient way to find out whether a generative model hasn't learned the true data distribution.

2.2 Annealed Importance Sampling

Calculating the LL of any decoder-based model involves calculating the following integral:

$$p_\theta(x) = \int p_\theta(x|z)p(z)dz \tag{2}$$

where $p(z)$ is the prior over the latent dimension and $p_\theta(x|z)$ is the probability of generating x, using the model, with the latent code z. Unfortunately, analytically solving this integral is intractable for complex decoder-based models. Instead, approximate methods such as Markov Chain Monte Carlo (MCMC) must be used in order to calculate the LL. In particular, Wu et al. showed that annealed importance sampling (AIS, Neal 2001) can be used to accurately approximate the LL of GANs.

AIS is an MCMC approach that uses multiple intermediate distributions in order to estimate the integral in equation 2. Wu et al. showed that an accurate estimate can be achieved, using many intermediate distributions (i.e. long MCMC chains) and multiple chains. When used to calculate the *log* of equation 2, the estimate is only a stochastic lower-bound (Grosse et al. 2015) of the LL that gets tighter as more intermediate distributions are introduced. For a more detailed explanation, see appendix A or Wu et al..

3   Are GANs Good Manifold Methods?

GANs transform samples from a low dimensional latent space, $\mathcal{Z}$, into the larger dimension of the data $\mathcal{X}$, effectively describing a manifold. In much of the literature, it is believed that the GAN captures the true low dimensional behavior of the training data (e.g. Menon et al.; Schlegl et al.; Xiao et al.; Bendel et al.; Schawinski et al.). A simple schematic of this assumption can be seen in figure 1, where it is usually expected that the images from the training distribution are very close to, or exactly on, the learned manifold. Furthermore, points that are not part of the training distribution are expected to be far from the learned manifold, whether they are natural images or not.

If GANs truly behave as believed and shown in figure 1, it should be possible to use them for classification and outlier detection (Schlegl et al. (2017)). For classification, an image is separately projected onto GANs trained on each of the classes and is classified according to the manifold whose projection was closest to the original image. Outlier detection can be carried out analogously, where the point is projected to the GAN manifold and if it's distance from the original point is too large it is deemed an outlier.

3.1   Inference with the GAN Manifold

We test whether modern GANs can be considered as manifold methods using a range of GANs and various datasets. The GANs we use are: StyleGAN-XL (Sauer et al. 2022) with an FID of 1.94 on ImageNet and 1.88 on CIFAR10, ReACGAN (Kang et al. 2021; 2022) with an FID of 8.19 on ImageNet and 3.87 on CIFAR10,
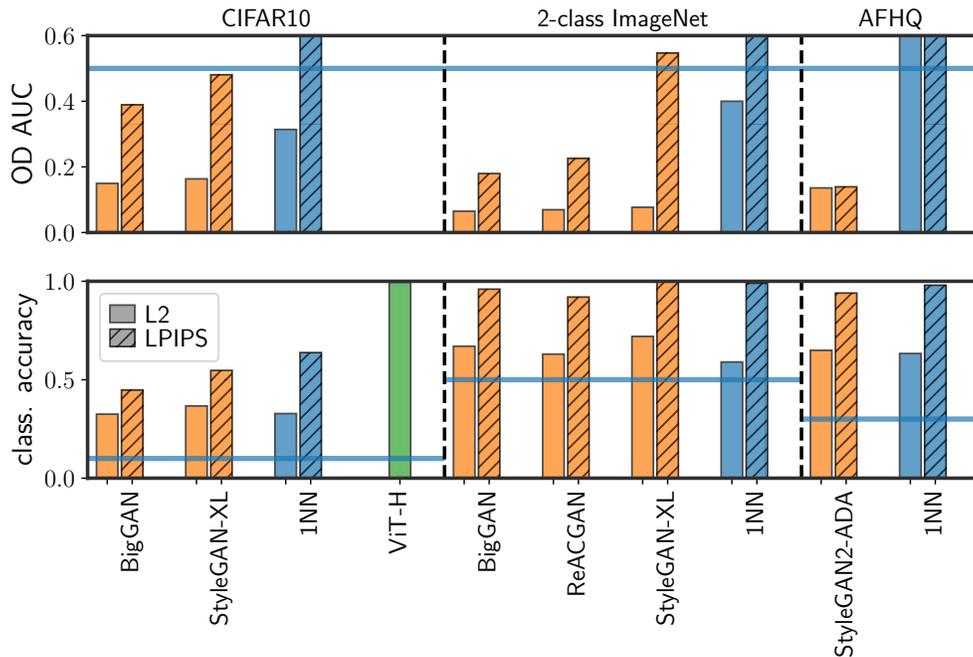
Figure 3: Performance of different GANs at the task of outlier detection (top) and classification (bottom). In all cases, both the ℓ_2 (plain) and the LPIPS (hatched, Zhang et al. 2018b) distances are used. The GANs are compared to a 1-nearest neighbor (1NN) baseline. For CIFAR10, all methods are also compared with ViT-H (Dosovitskiy et al. 2020). The GANs always underperform, compared to the 1NN baseline.

Figure 4: **Left:** ℓ_2 reconstruction errors (lower is better) for the reconstruction of different image groups by StyleGAN-XL trained on birds. The reconstruction error for birds or cars is similar, while there exist images that the GAN can reconstruct much better than those it was trained on. **Right:** examples for StyleGAN-XL reconstructions of car images and rescaled SVHN images. In all cases, the GANs capture the overall image structure, but don't retain the identity of the main object in the image, leading to projections which are far from the image whether in the training domain or not.

BigGAN-DiffAug (Zhao et al. 2020) with an FID of 8.7 on CIFAR10, BigGAN (Kang et al. 2022; Brock et al. 2018) with an FID of 8.54 on ImageNet, and StyleGAN2-ADA (Karras et al. 2020a) with an FID of 3.55 on AFHQCat and 7.4 on AFHQDog. To project the images on the GAN, we optimize the latent z code from multiple restarts and choose the optimized code with the smallest reconstruction error. Further details can be found in appendix B. All of the GANs chosen are able to generate highly realistic images and seemingly capture the full diversity of the datasets they were trained on.

In the task of classification, we analyze the performance of the GANs on a subset (1000 test samples) of the CIFAR10 dataset, a binary problem from ImageNet ("sports car" class versus the "blue heron" class) and a subset (1000) of AFHQ images, where the classes are AFHQDog, AFHQCat and AFHQWild. For outlier detection in all datasets, we consider images of a single color and rescaled versions of SVHN images as outliers and report the area under the ROC curve (OD AUC).

The first assumption we question is whether the GAN manifold actually passes through the training examples. For a given input x we can determine if it is on the GAN manifold by using gradient descent to approximately solve the optimization problem:

$$z^* = \arg\min_z \|G(z) - x\| \tag{3}$$

Surprisingly, it turns out that most of the training points are *not part of the GAN manifold.* Figure 2 (right) shows that for samples generated by the GAN, the optimization algorithm succeeds in finding a latent z so that the generated images is almost identical to the input image x. But for images from the training set, the best z found by the optimization algorithm generates an image that looks very different, although realistic. The figure also shows histograms of the reconstruction error of training samples found by inverting them from the $\mathcal{Z}$ space for StyleGAN-XL on ImageNet (for results on more GANs, see appendix C). As a baseline, samples generated by the GAN are also inverted and the histogram of their reconstruction error is shown as well. In general, the reconstruction error of training images is an order of magnitude worse than the reconstruction error of a generated image.

We then test the classification accuracy and outlier detection capabilities of the GANs. If the GANs have learned something close to the true data manifold, then they should act as good classifiers and outlier detectors. As a baseline, we compare the GANs to a simple 1-nearest-neighbor (1NN) estimator. Under the 1NN estimator, a sample is classified according to the class of its nearest neighbor. In outlier detection, a sample is considered an outlier if it is further than a pre-defined threshold from its nearest neighbor in the training distribution. This baseline is analogous to a GAN that has completely memorized the training examples and can't generate anything outside the training examples.

We again find that the learned manifolds do not behave as expected. Using the GAN manifolds for classification results in poor accuracy, as shown in figure 3 (bottom, in orange). The GANs are usually worse than the simple 1NN classifier (in blue), even when using a more perceptual distance such as LPIPS (Zhang et al. 2018b). The performance of GANs as outlier detectors is not much better, as shown in figure 3 (top) - the performance of most GANs is worse than random, even when using the perceptual distance. On the other hand, the 1NN outlier detector is always better than chance when using LPIPS.

We can better understand this poor performance by explicitly looking at the projections to the GAN manifold. Figure 4 (left) shows the reconstruction errors that different image groups have under a StyleGAN-XL trained on ImageNet blue heron (bird) images. Many images of sports cars have the same reconstruction error as images of birds, explaining why GANs are so bad at classifying between different images. Moreover, the GAN is able to reconstruct images of a single color and sometimes those from SVHN better than images from the distribution they were trained on. Figure 4 (right) shows projections of images of sports cars (top) and SVHN (bottom) onto the bird GAN. The projection of any image keeps the overall image structure, even for images from the wrong class. Because of this, the projection's distance from the original image is about the same whether the original was from the training distribution or not.

Such behavior is surprising. Images of sports cars and SVHN digits are frequently very different than those of blue herons, but the GAN is still able to reconstruct much of the context of the images. In images of cars, the GAN reconstruct the background, removing the car. For SVHN, the dominant colors and positions
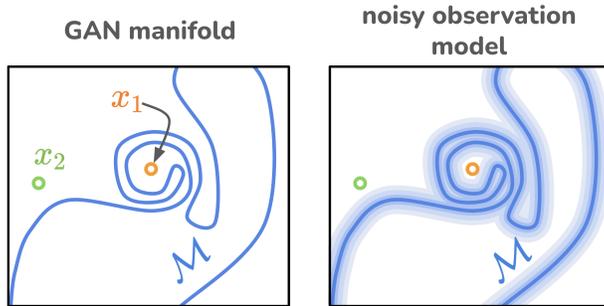
Figure 5: An example of a case where simply calculating the distance from the manifold might not tell the whole story. In this case, both x_1 and x_2 are the same distance from the manifold but the manifold is more abundant near x_1, making images in its region more plausible (left). By adding an observation model (right), queries to the model are transformed to calculating the log-likelihood under this observation model, essentially integrating over all possible areas of the manifold. With the observation model (right), x_1 is assigned a higher log-likelihood than x_2, even though they are equally distant from the manifold.

Model	Dataset	LL (bits/dim.) ↑	FID ↓
BigGAN-DiffAug	CIFAR10	-6.68	8.7
StyleGAN-XL	CIFAR10	-7.27	1.88
Glow (Kingma & Dhariwal, 2018)	CIFAR10	-3.35	3.35
DDPM++ (Song et al., 2020)	CIFAR10	-2.99	2.92
BigGAN	ImageNet	-7.59	8.54
StyleGAN-XL	ImageNet	-7.29	1.94
Glow (Kingma & Dhariwal, 2018)	ImageNet	-3.81	-
VDM (Kingma et al., 2021)	ImageNet	-3.4	-
StyleGAN2-ADA	AFHQ	-7.75	3.55

Table 1: GAN performance as a density estimator next to other generative models. Although GANs sometimes come ahead in terms of FID, their average test log-likelihood is always lower.

of the digits are kept. This is the same reconstruction behavior for images from the true distribution, an example of which can be seen in figure 2 (right) for training images.

4   Are GANs Good Density Estimators?

Viewing GANs purely as manifold methods potentially ignores two important aspects. First, the prior over the latent codes is completely ignored in all of the tests conducted above. Furthermore, while the GAN is equally far from points in or outside of the distribution, a larger portion of it might pass closer to the training samples than to other samples. An example of this can be seen in figure 5 (left): while both points are equally far from the manifold, more of the manifold passes close to the point in the middle of the spiral (x_1), and much less near the other point (x_2). Such behavior would explain why GANs are able to generate realistic images from the correct class while still being equally distant from points inside and out of the training distribution. To account for both of these aspects, we evaluate the GANs as density estimators, implicitly taking both the distribution over the latent space and the curvature of the manifold into account.

4.1   Adding an Observation Model

When distributions are defined on a low-rank space, it is common to assume an added "observation noise" (e.g. Wu et al. 2016; Kingma & Welling 2013; Tipping & Bishop 1999). In practice, this amounts to the generative model $x = G_\theta(z) + \text{noise}$ where the noise is often assumed to be Gaussian with a fixed variance,
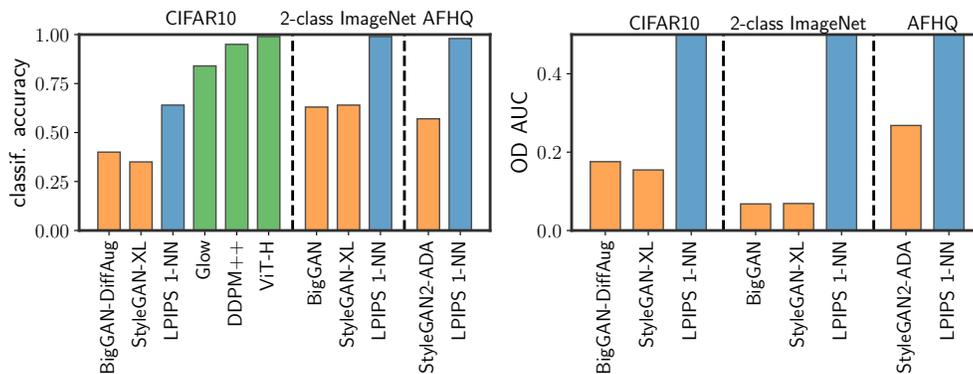
Figure 6: Performance of GANs as generative classifiers (left) and outlier detectors (right). The GANs are outperformed by simple baselines, as well as other generative models.

σ^2. The density (or likelihood) of a sample under the noisy model is then given by:

$$p_\theta(x) = \int p_\sigma \left(x | \ G_\theta(z) \right) p(z) dz \tag{4}$$

As mentioned by Wu et al., while the Gaussian observation model is possibly too simplistic, it can used to better understand the distributions learned by GANs. However, as long as this observation is used to compare GANs to each other, then we believe that it does give an indication of which GAN better captures the distribution.

We use the above described observation model in order to estimate the density GANs assign to previously unseen samples, conducting the same experiments as those for the manifold.

In all of our experiments, we use AIS with 500 steps, 4 chains, a Hamiltonian Monte Carlo (HMC) kernel and 10 leap-frogs to estimate a sample's LL. These values were chosen to mitigate the high computational load of running AIS while still extracting accurate estimates of the LL. More experimental details can be found in appendix B.1. The variance of the observation model was chosen to be the mean variance of the reconstruction error of training samples, which is the maximum likelihood estimator for the observation noise. In all cases, the PSNR of the images was high; that is, the variance of the noise assumed was much smaller than the strength of the signal. For more details regarding the variances used, see appendix B.3.

4.2   Evaluation as Density Models

Using the added observation model described above, we calculate the LL of the different GANs on unseen data and compare them to other generative models. This comparison can be found in table 1. GANs assign much lower LL to test samples than other methods, even when their FID is better than the other models.

Figure 6 shows the performance of the GANs as generative classifiers (left) and outlier detectors (right), next to the LPIPS 1NN baseline and other generative models. The classification accuracy of Glow is as reported by Fetaya et al. and that of DDPM++ as reported by Zimmermann et al.. Once again, the GANs are completely outperformed by the relatively simple 1NN estimator, indicating that the density GANs assign to samples is different than that of the true distribution.

Moreover, GANs tend to assign higher LL to images completely outside their training distribution, as can be seen in figure 7 (left): the StyleGAN-XL bird GAN gave higher LL to SVHN images than to test images.

To further understand the behavior of the GANs as density estimators, we look at which images have the highest and lowest LLs. The images with highest and lowest LLs from the "blue heron" class of ImageNet can be seen in figure 7 (center). Visually it seems that GANs prefer images with larger flat areas and low contrast. To be specific, figure 7 shows how the average coefficient of variance in small 8x8 patches of the image is anti-correlated with the LL (on the "sports car" and "blue heron" classes of ImageNet).
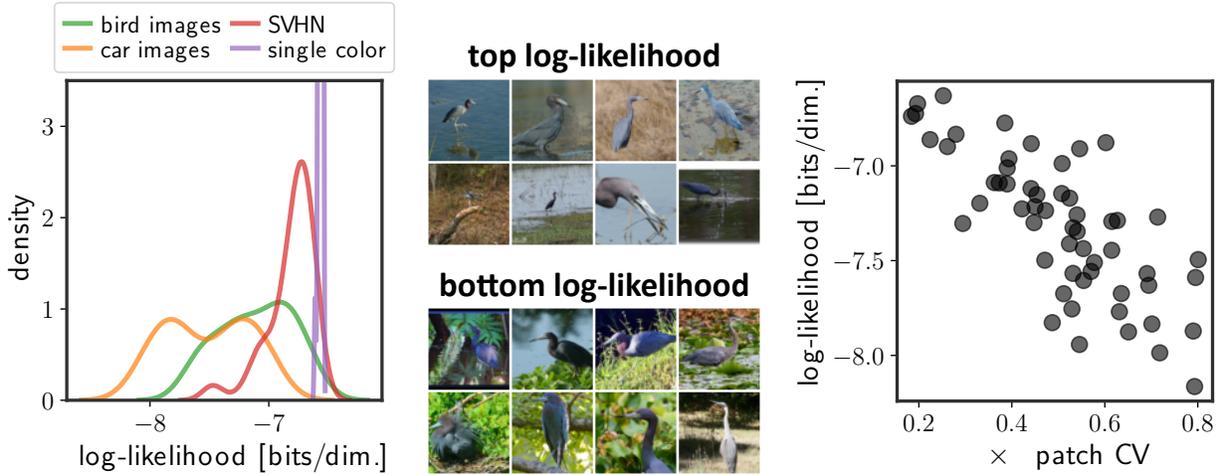
Figure 7: **Left:** log-likelihoods (higher is better) that different image groups attain under a StyleGAN-XL trained only on birds. Images of single color and SVHN images have higher log-likelihoods than images from the domain the GAN was trained on. **Middle:** the top and bottom images according to the log-likelihood. GANs tend to have a bias towards images with larger flat region. **Right:** a scatter plot of the images' log-likelihood against the average coefficient of variation (CV) of 8x8 patches. The log-likelihood assigned by the GAN is anti-correlated with the average variance of the patches in the image.

4.3 Typicality of Training Examples

While the samples from the true distribution might have lower LL than other sets of images, this alone is not an indication of a failure of the GAN. A stronger test is that of *typicality* of a set of images. For the distribution $p_\theta(x)$, we follow Nalisnick et al. and define the (ϵ, N)-typical set $\mathcal{A}_\epsilon^N(p_\theta)$ of the distribution as all sets of N samples that satisfy:

$$\left| \frac{1}{N} \sum_{i=1}^{N} \log p_\theta(x_i) + H(p_\theta) \right| \leq \epsilon \tag{5}$$

where $H(p_\theta)$ is the entropy of the distribution $p_\theta(x)$. When N is large, then (Cover 1999):

$$P\left(\mathcal{A}_\epsilon^N(p_\theta)\right) > 1 - \epsilon \tag{6}$$

That is, when N is large enough, this set of samples captures most of the distribution according to $p_\theta(x)$.

We begin by drawing i.i.d. samples from this typical set, i.e. we generate images from the GAN. We then calculate their LL using AIS, in exactly the same procedure as that for the training and SVHN images. The average LL of images generated by the GAN gives us an estimate of the entropy of $p_\theta(x)$: $\hat{H}(p_\theta) = -\frac{1}{N} \sum_{i=1}^{N} \log p_\theta(x)$ where $x_i \sim p_\theta(x)$. ϵ is chosen such that in 95% of the time, 50 samples drawn from the model are part of the typical set (i.e. the bootstrap confidence interval suggested by Nalisnick et al.).

Using the typicality test suggested by Nalisnick et al., we find that for the GANs we studied the set of *training samples is not part of the typical set* of the distribution defined by the GAN. Sometimes images from SVHN are even closer to being part of the typical set of the GAN than training images. This can be seen in figure 8 where histograms of the LLs for images generated by the GAN are shown next to histograms for other images. The dashed vertical lines are the means of the histograms for each image type and the shaded region is the ϵ-ball around the estimate of the entropy containing the typical sets $\mathcal{A}_\epsilon^N(p_\theta)$, according to a bootstrap estimator of ϵ. The mean LL for training images is always outside the shaded area, indicating that training images are not part of the typical sets of the GANs.
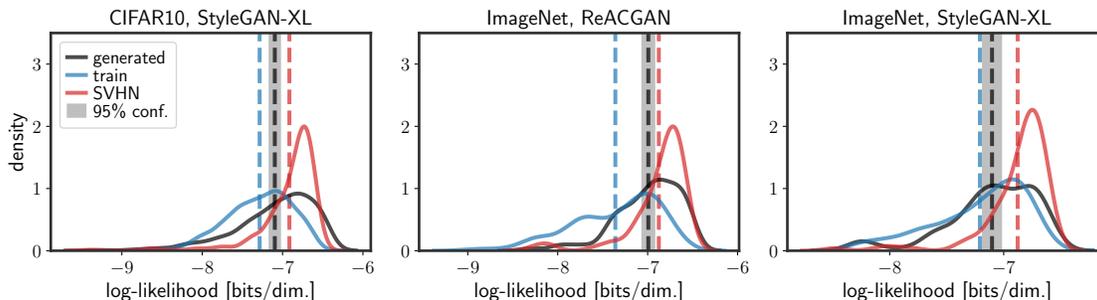
Figure 8: Histograms of log-likelihoods assigned to images generated by the GAN (black), train images (blue) and SVHN images (red). Each plot is for a different GAN-dataset pair. The dashed vertical lines are the means of the log-likelihood of the corresponding colored histogram, and the shaded area around the mean of the generated images are values of mean log-likelihoods associated with the typical set of the GAN. In all cases, the training images are outside this shaded area, meaning the set of training images *is not* part of the typical set of any of the GANs.

5 Related Works

This work follows a line of works (e.g. Nalisnick et al. 2018; Fetaya et al. 2019; Kirichenko et al. 2020) that show that many modern generative models do not truly capture the underlying data distribution. As far as we know, GANs have not been analyzed through the LL, despite their ability to generate images perceptually similar to natural images, as there is no direct access to the model likelihood.

There is a vast literature on evaluating whether GANs have learned the correct distribution (e.g. Heusel et al. 2017; Sajjadi et al. 2018; Ravuri & Vinyals 2019; Webster et al. 2019; Naeem et al. 2020; Borji 2022; Ravuri et al. 2023). Previous works predominantly use samples from the GAN in order to evaluate them, which raises some uncertainties because the space of all images is huge. In this work, we used the assumptions made when defining GANs in order to evaluate them, thereby side-stepping the issue of determining whether the learned distribution is correct through use of samples.

A key aspect of our investigation is the use of likelihood estimation and inference with GANs. There have been many works in the past that have suggested *extensions* to GANs in order to allow them to work as classifiers or outlier detectors (e.g. Schlegl et al. 2017; Donahue & Simonyan 2019; Kang et al. 2021; Nitzan et al. 2022). Other works change the definition of GANs in order to train them as density estimators together with their adversarial loss (Lucas et al. 2019; Abbasnejad et al. 2019). All such methods use an additional component besides the GAN generator, such as an encoder, which is not part of the generative process of the GAN. In this work, we utilize the above mentioned tasks as a way to better analyze how well the GAN has captured the true data distribution. We argue that if GANs accurately capture the true data distribution, their generator *alone* should be enough to achieve near-optimal performance in classification/outlier detection. Additionally, even with the added observation model, we should expect that the training images would be a part of the typical set of images supported by the GAN.

As mentioned in the introduction, GANs have been shown to not fully capture the training distribution in the past, especially due to "mode collapse" (Goodfellow 2016; Richardson & Weiss 2018). Arora et al. have quantified mode collapse by a "birthday paradox" test, in which they found that the support of many GANs is smaller than the size of the training distribution. To a large part, mode collapse seems not to be a problem of modern GANs which capture the full diversity of the training distribution, as evidenced by excellent FID scores. Instead, our analysis points to a deeper problem than previously investigated. Instead of fitting only small parts of the distribution, our results indicate that GANs misrepresent almost all parts of the distribution.

6 Discussion

Modern GANs are able to generate incredibly realistic images, that seem to arise from the same distribution as the images used to train the GAN. Moreover, they have excellent performance under modern evaluation metrics. These facts have led to a common belief that GANs capture the true data manifold and the true data distribution.

When analyzing GANs as manifold methods, we find that their manifolds do not fit the training samples. Quantitatively, this failure can be summarized by the classification and outlier detection performance of the GANs when defining the distance from the manifold as an estimate for whether the sample is from the GAN's distribution or not. Even when relaxing the requirement that samples should be part of the GAN manifold does not improve the situation, as is evidenced by the poor generative classification behavior. Worse, we showed how the training examples are not part of the typical set of the GAN.

Even though this work has presented an overall negative view of GANs, they are still extremely powerful data samplers. Indeed, this fact was taken advantage of in domains such as image manipulation, style transfer and data augmentation, to great effect. However, our work shows that a more cautious stance should be taken when attempting to use GANs as priors for the true data distribution.

References

M Ehsan Abbasnejad, Qinfeng Shi, Anton van den Hengel, and Lingqiao Liu. A generative adversarial density estimator. In *Proceedings of the IEEE/CVF Conference on Computer Vision and Pattern Recognition*, pp. 10782–10791, 2019.

Sanjeev Arora, Andrej Risteski, and Yi Zhang. Do gans learn the distribution? some theory and empirics. In *International Conference on Learning Representations*, 2018.

Matthew Bendel, Rizwan Ahmad, and Philip Schniter. A regularized conditional gan for posterior sampling in inverse problems. *arXiv preprint arXiv:2210.13389*, 2022.

Ali Borji. Pros and cons of gan evaluation measures: New developments. *Computer Vision and Image Understanding*, 215:103329, 2022.

Andrew Brock, Jeff Donahue, and Karen Simonyan. Large scale gan training for high fidelity natural image synthesis. *arXiv preprint arXiv:1809.11096*, 2018.

Thomas M Cover. *Elements of information theory*. John Wiley & Sons, 1999.

Jeff Donahue and Karen Simonyan. Large scale adversarial representation learning. *Advances in neural information processing systems*, 32, 2019.

Alexey Dosovitskiy, Lucas Beyer, Alexander Kolesnikov, Dirk Weissenborn, Xiaohua Zhai, Thomas Unterthiner, Mostafa Dehghani, Matthias Minderer, Georg Heigold, Sylvain Gelly, et al. An image is worth 16x16 words: Transformers for image recognition at scale. *arXiv preprint arXiv:2010.11929*, 2020.

Richard O Duda, Peter E Hart, and David G Stork. *Pattern classification and scene analysis*, volume 3. Wiley New York, 1973.

Ethan Fetaya, Jörn-Henrik Jacobsen, Will Grathwohl, and Richard Zemel. Understanding the limitations of conditional generative models. *arXiv preprint arXiv:1906.01171*, 2019.

Ian Goodfellow. Nips 2016 tutorial: Generative adversarial networks. *arXiv preprint arXiv:1701.00160*, 2016.

Ian Goodfellow, Jean Pouget-Abadie, Mehdi Mirza, Bing Xu, David Warde-Farley, Sherjil Ozair, Aaron Courville, and Yoshua Bengio. Generative adversarial nets. *Advances in neural information processing systems*, 27, 2014.

Roger B Grosse, Zoubin Ghahramani, and Ryan P Adams. Sandwiching the marginal likelihood using bidirectional monte carlo. *arXiv preprint arXiv:1511.02543*, 2015.

Martin Heusel, Hubert Ramsauer, Thomas Unterthiner, Bernhard Nessler, and Sepp Hochreiter. Gans trained by a two time-scale update rule converge to a local nash equilibrium. *Advances in neural information processing systems*, 30, 2017.

Geoffrey E Hinton, Peter Dayan, Brendan J Frey, and Radford M Neal. The" wake-sleep" algorithm for unsupervised neural networks. *Science*, 268(5214):1158–1161, 1995.

Minguk Kang, Woohyeon Shim, Minsu Cho, and Jaesik Park. Rebooting acgan: Auxiliary classifier gans with stable training. *Advances in neural information processing systems*, 34:23505–23518, 2021.

Minguk Kang, Joonghyuk Shin, and Jaesik Park. Studiogan: a taxonomy and benchmark of gans for image synthesis. *arXiv preprint arXiv:2206.09479*, 2022.

Minguk Kang, Jun-Yan Zhu, Richard Zhang, Jaesik Park, Eli Shechtman, Sylvain Paris, and Taesung Park. Scaling up gans for text-to-image synthesis. In *Proceedings of the IEEE/CVF Conference on Computer Vision and Pattern Recognition*, pp. 10124–10134, 2023.

Tero Karras, Miika Aittala, Janne Hellsten, Samuli Laine, Jaakko Lehtinen, and Timo Aila. Training generative adversarial networks with limited data. *Advances in neural information processing systems*, 33: 12104–12114, 2020a.

Tero Karras, Samuli Laine, Miika Aittala, Janne Hellsten, Jaakko Lehtinen, and Timo Aila. Analyzing and improving the image quality of stylegan. In *Proceedings of the IEEE/CVF conference on computer vision and pattern recognition*, pp. 8110–8119, 2020b.

Tero Karras, Miika Aittala, Samuli Laine, Erik Härkönen, Janne Hellsten, Jaakko Lehtinen, and Timo Aila. Alias-free generative adversarial networks. *Advances in Neural Information Processing Systems*, 34: 852–863, 2021.

Diederik Kingma, Tim Salimans, Ben Poole, and Jonathan Ho. Variational diffusion models. *Advances in neural information processing systems*, 34:21696–21707, 2021.

Diederik P Kingma and Max Welling. Auto-encoding variational bayes. *arXiv preprint arXiv:1312.6114*, 2013.

Durk P Kingma and Prafulla Dhariwal. Glow: Generative flow with invertible 1x1 convolutions. *Advances in neural information processing systems*, 31, 2018.

Polina Kirichenko, Pavel Izmailov, and Andrew G Wilson. Why normalizing flows fail to detect out-of-distribution data. *Advances in neural information processing systems*, 33:20578–20589, 2020.

Tuomas Kynkäänniemi, Tero Karras, Samuli Laine, Jaakko Lehtinen, and Timo Aila. Improved precision and recall metric for assessing generative models. *Advances in Neural Information Processing Systems*, 32, 2019.

Thomas Lucas, Konstantin Shmelkov, Karteek Alahari, Cordelia Schmid, and Jakob Verbeek. Adaptive density estimation for generative models. *Advances in Neural Information Processing Systems*, 32, 2019.

Sachit Menon, Alexandru Damian, Shijia Hu, Nikhil Ravi, and Cynthia Rudin. Pulse: Self-supervised photo upsampling via latent space exploration of generative models. In *Proceedings of the ieee/cvf conference on computer vision and pattern recognition*, pp. 2437–2445, 2020.

Muhammad Ferjad Naeem, Seong Joon Oh, Youngjung Uh, Yunjey Choi, and Jaejun Yoo. Reliable fidelity and diversity metrics for generative models. In *International Conference on Machine Learning*, pp. 7176–7185. PMLR, 2020.

Eric Nalisnick, Akihiro Matsukawa, Yee Whye Teh, Dilan Gorur, and Balaji Lakshminarayanan. Do deep generative models know what they don't know? *arXiv preprint arXiv:1810.09136*, 2018.

Eric Nalisnick, Akihiro Matsukawa, Yee Whye Teh, and Balaji Lakshminarayanan. Detecting out-of-distribution inputs to deep generative models using typicality. *arXiv preprint arXiv:1906.02994*, 2019.

Radford M Neal. Annealed importance sampling. *Statistics and computing*, 11:125–139, 2001.

Yotam Nitzan, Rinon Gal, Ofir Brenner, and Daniel Cohen-Or. Large: Latent-based regression through gan semantics. In *Proceedings of the IEEE/CVF Conference on Computer Vision and Pattern Recognition*, pp. 19239–19249, 2022.

Suman Ravuri and Oriol Vinyals. Classification accuracy score for conditional generative models. *Advances in neural information processing systems*, 32, 2019.

Suman Ravuri, Mélanie Rey, Shakir Mohamed, and Marc Peter Deisenroth. Understanding deep generative models with generalized empirical likelihoods. In *Proceedings of the IEEE/CVF Conference on Computer Vision and Pattern Recognition*, pp. 24395–24405, 2023.

Eitan Richardson and Yair Weiss. On gans and gmms. *Advances in neural information processing systems*, 31, 2018.

Mehdi SM Sajjadi, Olivier Bachem, Mario Lucic, Olivier Bousquet, and Sylvain Gelly. Assessing generative models via precision and recall. *Advances in neural information processing systems*, 31, 2018.

Axel Sauer, Katja Schwarz, and Andreas Geiger. Stylegan-xl: Scaling stylegan to large diverse datasets. In *ACM SIGGRAPH 2022 conference proceedings*, pp. 1–10, 2022.

Kevin Schawinski, Ce Zhang, Hantian Zhang, Lucas Fowler, and Gokula Krishnan Santhanam. Generative adversarial networks recover features in astrophysical images of galaxies beyond the deconvolution limit. *Monthly Notices of the Royal Astronomical Society: Letters*, 467(1):L110–L114, 2017.

Thomas Schlegl, Philipp Seeböck, Sebastian M Waldstein, Ursula Schmidt-Erfurth, and Georg Langs. Unsupervised anomaly detection with generative adversarial networks to guide marker discovery. In *International conference on information processing in medical imaging*, pp. 146–157. Springer, 2017.

Yang Song, Jascha Sohl-Dickstein, Diederik P Kingma, Abhishek Kumar, Stefano Ermon, and Ben Poole. Score-based generative modeling through stochastic differential equations. *arXiv preprint arXiv:2011.13456*, 2020.

Lucas Theis, Aäron van den Oord, and Matthias Bethge. A note on the evaluation of generative models. *arXiv preprint arXiv:1511.01844*, 2015.

Michael E Tipping and Christopher M Bishop. Principal component analysis. 1999.

Ryan Webster, Julien Rabin, Loic Simon, and Frédéric Jurie. Detecting overfitting of deep generative networks via latent recovery. In *Proceedings of the IEEE/CVF Conference on Computer Vision and Pattern Recognition*, pp. 11273–11282, 2019.

Yuhuai Wu, Yuri Burda, Ruslan Salakhutdinov, and Roger Grosse. On the quantitative analysis of decoder-based generative models. *arXiv preprint arXiv:1611.04273*, 2016.

Zhisheng Xiao, Karsten Kreis, and Arash Vahdat. Tackling the generative learning trilemma with denoising diffusion gans. *arXiv preprint arXiv:2112.07804*, 2021.

Mengshi Zhang, Yuqun Zhang, Lingming Zhang, Cong Liu, and Sarfraz Khurshid. Deeproad: Gan-based metamorphic testing and input validation framework for autonomous driving systems. In *Proceedings of the 33rd ACM/IEEE International Conference on Automated Software Engineering*, pp. 132–142, 2018a.

Richard Zhang, Phillip Isola, Alexei A Efros, Eli Shechtman, and Oliver Wang. The unreasonable effectiveness of deep features as a perceptual metric. In *Proceedings of the IEEE conference on computer vision and pattern recognition*, pp. 586–595, 2018b.

Shengyu Zhao, Zhijian Liu, Ji Lin, Jun-Yan Zhu, and Song Han. Differentiable augmentation for data-efficient gan training. *Advances in Neural Information Processing Systems*, 33:7559–7570, 2020.

Roland S Zimmermann, Lukas Schott, Yang Song, Benjamin A Dunn, and David A Klindt. Score-based generative classifiers. *arXiv preprint arXiv:2110.00473*, 2021.

A Brief Explanation of the AIS Algorithm

Let $f(z)$ be a target un-normalized distribution. An AIS chain is defined by an initial distribution $Q_0(z) = q_0(z)/Z_0$ whose normalization coefficient is known, together with T intermediate distributions $Q_1(z), \cdots, Q_T(Z)$ such that $Q_T(z) = q_T(z)/Z_T = f(z)/Z_T$. Each step of the chain further requires an MCMC transition operator $\mathcal{T}_t$ which keeps $Q_t(z)$ invariant, such as Hamiltonian Monte-Carlo (HMC). Beginning with a sample from the initial distribution $z_0 \sim Q_0(z)$ and setting $w_0 = 1$, AIS iteratively carries out the following steps:

$$w_t = w_{t-1} \cdot \frac{q_t(z_{t-1})}{q_{t-1}(z_{t-1})} \qquad\qquad z_t \sim \mathcal{T}_t\left(z | z_{t-1}\right) \tag{7}$$

The importance weights w_T aggregated during the sampling procedure are an unbiased estimate of the ratio of normalizing coefficients, such that $\mathbb{E}\left[w_T\right] = Z_T/Z_0$.

Given a sample x, the likelihood can be calculated through AIS by setting $f(z) = p(z)p_\theta(x|z)$ as the target distribution, such that $p_\theta(x)$ is the corresponding normalization constant $\mathcal{Z}_T$. In practice, the likelihood is estimated in log-space to avoid numerical difficulties such as underflows. Calculating the log of the importance weights as described above is straightforward, however Grosse et al. have shown that doing so results in a stochastic lower bound of the log-likelihood. As the number of intermediate steps T increases, this stochastic lower bound becomes tighter and converges to the true log-likelihood.

B Implementation Details

B.1 AIS Details

We follow the implementation of AIS from Wu et al. (publicly available in GitHub), reimplemented in PyTorch. When possible, we used the same settings as Wu et al.:

- The transition operator we used was HMC with 10 leapfrog steps and a Metropolis-Hastings (MH) adjustment. During sampling, the learning rate is initialized to $5 \cdot 10^{-2}$ and adjusted according to a moving average of the MH rejection rate

- During sampling, the intermediate distributions we used were:

$$Q_t(z) \propto p(z) \cdot p_\gamma\left(x|\ G_\theta(z)\right)^{\beta_t} \tag{8}$$

  β_t was annealed according to a sigmoidal schedule

Choice of Number of Steps The bound on the log-likelihood approximated by AIS becomes tight and accurate only as the number of intermediate distribution and number of chains grows, respectively. However, AIS with many chains and intermediate distributions is incredibly computationally costly. Due
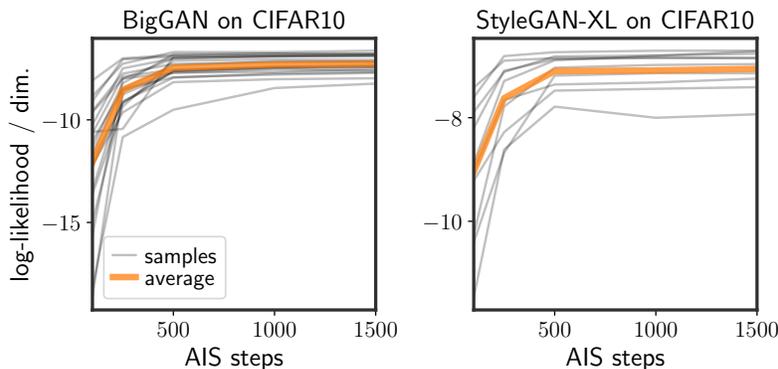
Figure 9: The estimated log-likelihood as a function of AIS steps, for different GANs on CIFAR10 on random test samples. The log-likelihood of most samples converges after 500 steps.

to these considerations we use a relatively small number of intermediate distributions, while still ensuring accurate enough results.

Each chain used 500 intermediate steps. This number is in stark contrast to the 10,000 iterations used by Wu et al.. We chose this number by running multiple AIS chains with a differing number of intermediate steps, plotting the estimated log-likelihood as a function of AIS steps, as shown in Figure 9. The estimated log-likelihood typically stabilizes very close to the value reached after 500 iterations. The difference between the converged value and the one after 500 steps is much smaller than the resolution of log-likelihoods we are looking at, so this is a compromise between accuracy and computational cost.

Further justification for this is due to the comparison between AIS and GAN inversion in terms of gradient steps. Because of the leapfrog steps, a single iteration of AIS is similar to 10 gradient steps in GAN inversion. In all of our experiments, $\sim$750 iterations were enough to converge during inversion, well below the 5000 gradient steps used during the AIS procedure.

B.2 Reconstruction through GAN Inversion

There is a vast literature on the best way to reconstruct test images using GANs, also called *GAN inversion.* In this work we used a simple, albeit rather costly, approach in order to find the best possible reconstruction.

We used an optimization approach towards GAN inversion, using ADAM as the optimizer and a cosine schedule (similar to the scheme used by Sauer et al. in their implementation) for $\sim 500 - 750$ iterations (which we found to usually be many more iterations than required). To find better reconstructions, we sampled ~ 500 images from the GAN and initialized the optimizer from the latent code of the image closest to the input image in ℓ_2 distance. Furthermore, this process was repeated ~ 4 times for each image. Using this GAN inversion scheme, we were typically able to invert images generated by the GAN (and frequently images of a single color as well).

Finally, note that for all experiments with the StyleGAN variants, the inversion took place in $\mathcal{Z}$ space, as the generative model is defined in terms of this latent space and not the $\mathcal{W}/\mathcal{W}+$ spaces.

B.3 Observation Model

To calculate the GANs' density, we assumed an additive Gaussian noise observation model, with the same variance σ^2 for all samples. This observation model was used by Wu et al. among others. The values of σ^2 and their respective PSNR can be found in Table 2. As mentioned in the main body of text, the value of σ^2 used was the variance of the GAN's reconstruction error. This choice of σ^2 maximizes the likelihood the model gives to training data.

15

GAN	Dataset	Value of σ^2	PSNR
BigGAN	CIFAR10	0.008	21.2
StyleGAN-XL	CIFAR10	0.018	17.4
BigGAN	ImageNet10	0.012	19.2
StyleGAN-XL	ImageNet10	0.021	16.8
StyleGAN2-ADA	AFHQ	0.019	17.2

Table 2: Table of variances used for σ^2 throughout the paper and their respective PSNR.
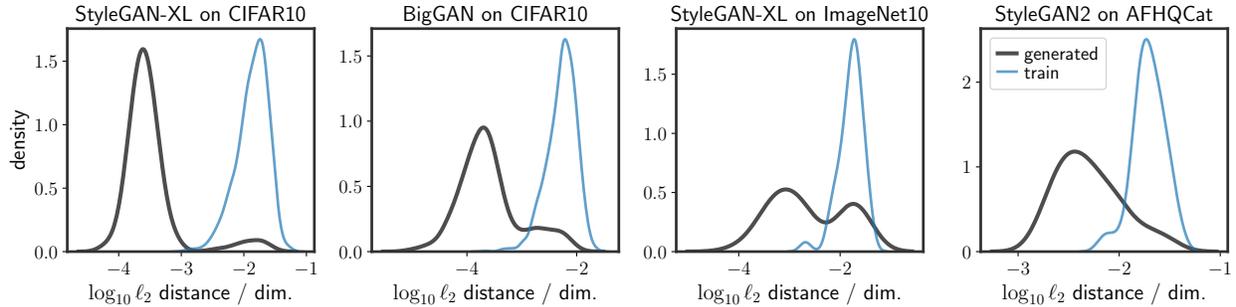

Figure 10: Log reconstruction errors of training vs generated examples for more GANs. In all cases, the distribution of the training examples is different than of the generated examples. The plot for StyleGAN-XL on ImageNet is on a bigger subset of ImageNet classes than in figure 2, showing that this result is broader than the 2 classes discussed in the main body of text.

C More Results

Figure 10 shows more histograms of the reconstruction errors for training examples vs. images generated by GANs. In all cases, the distribution of the reconstruction errors is different for train and generated examples, indicating that for all GANs examined the training samples are not on the GAN manifold.

Figure 11 shows more examples of reconstructions.

Figure 12 shows LL histograms for different image groups under different GANs.
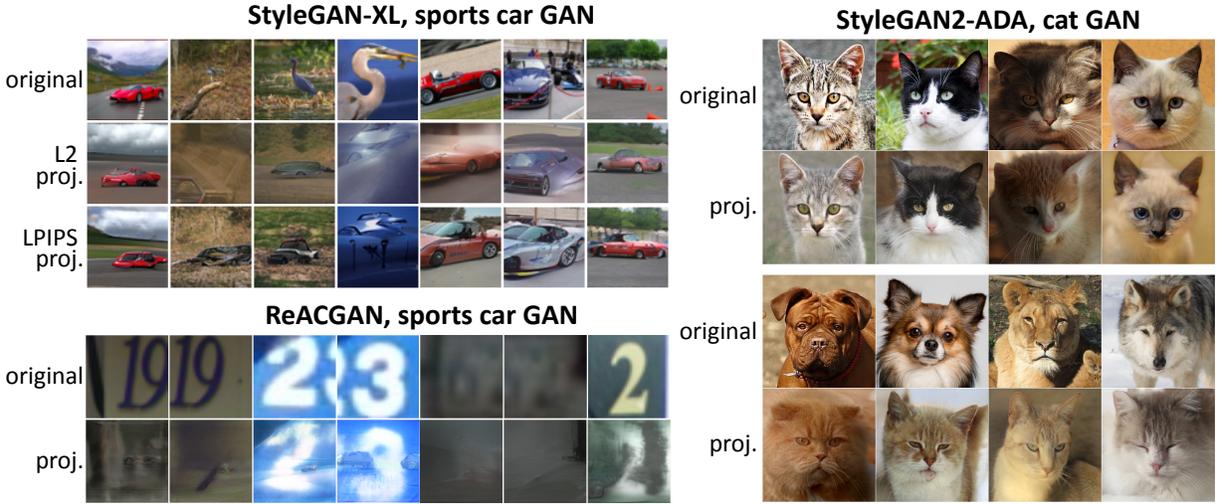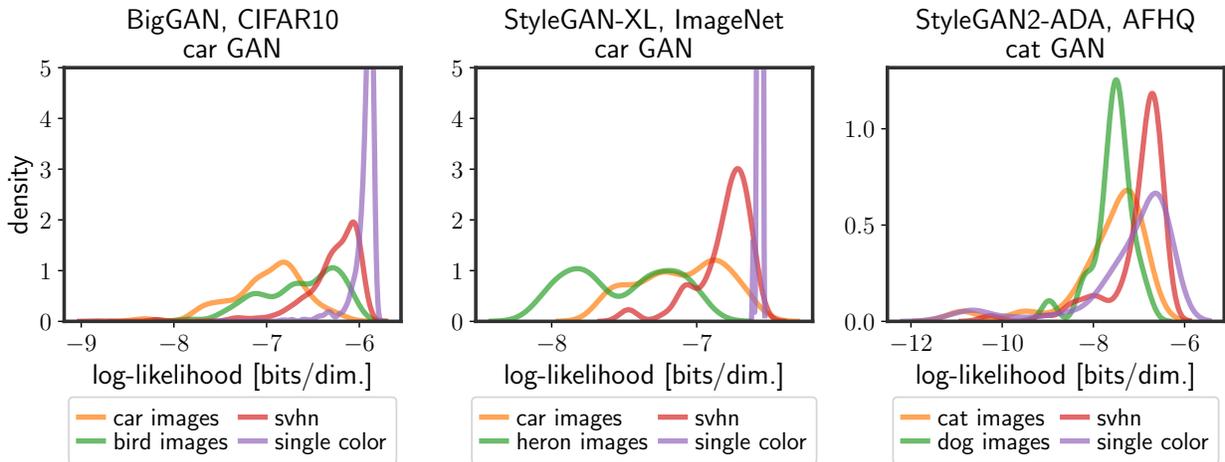
Figure 11: More GAN inversions.

Figure 12: Histograms of LLs for more GANs than shown in the main text.